Insertion and Removal of Protons in Single-Crystal Orthorhombic Molybdenum Trioxide under H_2S/H_2 and O_2/N_2

H. C. Zeng,*,† F. Xie,† K. C. Wong,‡ and K. A. R. Mitchell*,‡

Department of Chemical and Environmental Engineering, Faculty of Engineering, National University of Singapore, 10 Kent Ridge Crescent, Singapore 119260, and Department of Chemistry, University of British Columbia, 2036 Main Mall, Vancouver, British Columbia, V6T 1Z1, Canada

Received October 16, 2001. Revised Manuscript Received January 9, 2002

Using AFM/XRD/XPS methods, in this paper, we investigate protonation and deprotonation processes in single-crystal samples of orthorhombic molybdenum trioxide (α-MoO_3). At low temperatures, a small part of α-MoO_3 is changed to needlelike H_xMoO_3 ($x \approx 0.33$) along ⟨203⟩ directions in a H_2S/H_2 gas stream. When these elongated crystallites assemble into a maze structure, the growth of H_xMoO_3 is gradually ceased due to closing entrance for hydrogen. At higher temperatures, the needlelike H_xMoO_3 crystallites turn to a growth perpendicular to ⟨203⟩, which leads to the formation of H_xMoO_3 blocks. It is observed that the basal plane of α-MoO_3 is severely buckled upon the protonation. Surface sulfidation is also observed. The formed H_xMoO_3 or surface MoS_2, however, can be readily converted back to their original-phase α-MoO_3 in air at 350−400 °C. This oxidation process gives rise to a flattened (010) topography (i.e., debuckling) on which shallowly divided α-MoO_3 surface blocks bounded with {101} planes are formed. When an α-MoO_3 (010) plane embedded with nanocrystallites is used to create surface stress or nucleation sites, the insertion mode of hydrogen along ⟨001⟩ is further reconfirmed in this work. A correlation of surface/bulk phases upon various chemical reactions is addressed, and a model to summarize these changes is also proposed.

Introduction

Layered transition metal oxides have attracted great research attention owing to their many important applications over the past decades.[1−15] These materials have long been known as catalytic materials in molecular hydrogenation, dehydrogenation, epoxidation, isomerization, disproportionation, polymerization, etherification, addition, and dehydrogenation.[1−8] In recent years, these materials have also been used as electronic and structural materials in many new applications.[9−15] For instance, nanometer-sized molybdenum trioxide MoO_3 has been investigated for its outstanding performance in load-independent friction application.[12] Tungsten trioxide WO_3 together with MoO_3, on the other hand, have been used as host materials and studied for their photochromic and electrochromic properties for use in information display, sensor devices, and "smart windows".[14]

The underlying sciences of the above widely covered applications are based on unique structural and electronic properties of this class of materials. In particular, multiple oxidation states of transition metal cations and highly anisotropic structures when they are combined with oxygen anions are the two primary properties governing these applications.[1−15] In orthorhombic form of MoO_3 (α-MoO_3), as an example, there are three different types of oxygen atoms in association with molybdenum.[16,17] First, there is a terminal oxygen

* To whom correspondence should be addressed.
† National University of Singapore.
‡ University of British Columbia.

(1) Haber, J. In *Molybdenum: An Outline of Its Chemistry and Uses*; Braithwaite, E. R., Haber, J., Eds.; Elsevier Science: Amsterdam, 1994; Chapter 10, p 479.
(2) Haber, J.; Lalik, E. *Catal. Today* **1997**, *33*, 119.
(3) Zhang, C. M.; Chen, S. Y.; Yang, Z. P.; Peng, S. Y. In *Sol−Gel Processing and Applications*; Attia, Y. A., Ed.; Plenum Press: New York, 1994; p 379.
(4) Hayashi, H.; Sugiyama, S.; Masaoka, N.; Shigemoto, N. *Ind. Eng. Chem. Res.* **1995**, *34*, 137.
(5) Sabu, K. R.; Rao, K. V.; Nair, C. G. R. *Indian J. Chem.* **1994**, *33B*, 1053.
(6) Fournier, M.; Aouissi, A.; Rocchiccioli-Deltcheff, C. *J. Chem. Soc., Chem. Commun.* **1994**, (3), 307.
(7) Günther, S.; Marsi, M.; Kolmakov, A.; Kiskinova, M.; Noeske, M.; Taglauer, E.; Mestl, G.; Schubert, U. A.; Knozinger, H. *J. Phys. Chem. B* **1997**, *101*, 10004.
(8) Takenaka, S.; Tanaka, T.; Funabiki, T.; Yoshida, S. *J. Phys. Chem. B* **1998**, *102*, 2960.
(9) Haber, J. In *Molybdenum: An Outline of Its Chemistry and Uses*; Braithwaite, E. R., Haber, J., Eds.; Elsevier Science: Amsterdam, 1994; Chapter 10, p 494.
(10) Thorne, R. E. *Phys. Today* **1996**, *49*, 42.
(11) Tagaya, H.; Ara, K.; Kadokawa, J. I.; Karasu, M.; Chiba, K. *J. Mater. Chem.* **1994**, *4*, 551.
(12) Wang, J.; Rose, K. C.; Lieber, C. M. *J. Phys. Chem. B* **1999**, *103*, 8405.
(13) Carcia, P. F.; McCarron, E. M., III. *Thin Solid Films* **1987**, *155*, 53.
(14) Yang, Y. A.; Cao, Y. W.; Loo, B. H.; Yao, J. N. *J. Phys. Chem. B* **1998**, *102*, 9392 and the references therein.
(15) Kerr, T. A.; Leroux, F.; Nazar, L. F. *Chem. Mater.* **1998**, *10*, 2588.
(16) Kihlborg, L. *Arkiv. Kemi* **1963**, *21*, 357.

10.1021/cm011506z CCC: $22.00
Published on Web 03/08/2002

Table 1. Reaction Conditions for the Protonation and Depotonation Experiments.

proton insertion reactions	
temperature range	125−300 °C
reaction time	0.5−3 h
gas flow rate	20−30 mL/min
H_2S in H_2	5−20 mol %
proton removal reactions	
temperature range	350−400 °C
reaction time	1−3 h
reaction atmosphere	static laboratory air

bonded to only one Mo atom with a distance of 1.67 Å. Second, there are symmetrically bridging-oxygen atoms bonded to two Mo atoms with a bond length at 1.95 Å (×2) and weakly linked to a third Mo atom at 2.33 Å. Finally, there are two asymmetric bridging-oxygen atoms connected to two Mo atoms with bond lengths at 1.74 and 2.25 Å, respectively.[16,17] With these six Mo−O bonds, a Mo atom is essentially located in a distorted octahedron. When these MoO_6 octahedra are edge-connected along ⟨001⟩ and corner-linked along ⟨100⟩ , a double-layer structure is formed and, through van der Waals forces, an alternative stack of these double layers (or basal layers) along ⟨010⟩ will lead to a three-dimensional structure of α-MoO_3.[16−18]

One of the most important properties of α-MoO_3 is its cation intercalation ability. In forming molybdenum bronzes A_xMoO_3 (A = monovalent cations such as proton and alkali ions), the oxidation state of Mo^{VI} must be partially reduced.[19−29] There have been numerous investigations in this area regarding the structural and electronic properties of pure-phase A_xMoO_3 in which the synthesis of A_xMoO_3 is normally started from MoO_3 powders.[19−26] Very recently, single-crystal α-MoO_3 has been used to investigate partial oxidation of alcohols at 200−400 °C.[27,28] Surprisingly, acicular hydrogen molybdenum bronze H_xMoO_3 along ⟨203⟩ has been formed topotactically on the {010} surface of α-MoO_3 in nitrogen-alcohol (methanol, ethanol, and 2-propanol) atmospheres.[27,28] Related to general protonation processes, the hydrogen insertion direction in an α-MoO_3 host matrix at reaction temperatures of ≈150 °C using a gas stream of $H_2S + H_2$ was recently explored by us.[29] In this paper, we will use single crystals of α-MoO_3 to investigate the protonation and depotonation processes using the same gas stream for the reactions at different temperatures. In particular, fundamental issues such as surface stresses and H_xMoO_3 growth, insertion reversibility of protons, and sulfidation/oxidation reactions among various surface phases will be addressed with AFM, XRD, and XPS methods. Our new findings show that previously reported acicular H_xMoO_3 crystals can be further grown perpendicular to ⟨203⟩, leading to the formation of H_xMoO_3 blocks. When the intercalated protons are removed (i.e., oxidized in air), the reacted α-MoO_3 matrix returns to its original form except that the topmost surface layers have been reconstructed to blocks bounded with {101} planes.

Experimental Section

The host material α-MoO_3 for proton insertion and removal was prepared according to a previously developed flux-growth method. Briefly, single crystals of α-MoO_3 with smooth morphology were prepared with a high-temperature flux (the mole ratio of MoO_3:Na_2MoO_4 = 85:15) at a cooling rate of 2 °C/h.[30] The platelike α-MoO_3 single crystals were separated from the solid-solvent Na_2MoO_4 by using a dilute nitric acid solution (1.0 M). For protonation and deprotonation experiments, typically, a high-quality α-MoO_3 sample with the size of 10 mm (in [001]) × 3 mm (in [100]) × 0.5 mm (in [010]) was selected and cut from a large single crystal (transparent) with the aid of an optical microscope (Olympus BH-2). The H + MoO_3 reaction was carried out in a glass reactor at 125−300 °C using a H_2S stream (5−20 mol % H_2S, balanced with H_2) under atmospheric pressure. The temperature of the reactor was monitored continuously with a K-type thermocouple. A small flow rate of 20−30 mL/min (controlled by a mass-flow control system, Brooks 5950) in the input stream (versus the large reactor volume = 250 mL) was to ensure that there was no concentration gradient of H_2S across the reactor. The off-gas was introduced to a $ZnSO_4$ solution to remove unreacted H_2S before it was vented into the atmosphere. In the deprotonation reaction, the above H-inserted α-MoO_3 (or H_xMoO_3) was further heat-treated in an electric furnace (Carbolite) with the static laboratory air (i.e., O_2/N_2) at various temperatures. Further details of these reaction experiments can be found in Table 1.

Crystallographic information of the above-reacted samples was investigated with X-ray diffraction (XRD; Shimadzu XRD-6000, Cu Kα radiation, λ = 1.5406 Å).[31] The surface topography of the samples was examined with an atomic force microscope (AFM; DI NanoScope MultiMode) in tapping mode to minimize damage of the stepped surfaces by the single-crystal silicon probe. The typical scan size in this work was set as 8 × 8 μm. On average, AFM images from more than four sampling locations per sample were recorded to ensure a good representation of the surface topography.[18] The surface chemical analysis of reacted samples was made with X-ray photonelectron spectroscopy (XPS; Leybold MAX200) method using Al Kα X-ray source ($h\nu$ = 1486.6 eV).[32] The XPS spectra of all studied elements such as C 1s, O 1s, S 2p, and Mo 3d were measured with a constant analyzer pass energy of 48 eV. All binding energies (BEs) were referenced to the C 1s peak (BE = 284.7 eV) arising from adventitious carbon. Prior to peak deconvolution, inelastic background (Shirley-type) was subtracted for all XPS spectra.

Results and Discussion

Proton Insertion and Formation of Acicular H_xMoO_3. After protonation reactions, the α-MoO_3 crys-

(17) (a) Chen, M.; Waghmare, U. V.; Friend, C. M.; Kaxiras, E. *J. Chem. Phys.* **1998**, *109*, 6854. (b) Queeney, K. T.; Friend, C. M. *J. Phys. Chem. B* **2000**, *104*, 409.
(18) Hsu, Z. Y.; Zeng, H. C. *J. Phys. Chem. B* **2000**, *104*, 11891.
(19) Dickens, P. G.; Birtill, J. J.; Wright, C. J. *J. Solid State Chem.* **1979**, *28*, 185.
(20) Slade, R. C. T.; Halstead, T. K.; Dickens, P. G. *J. Solid State Chem.* **1980**, *34*, 183.
(21) Dickens, P. G.; Crouch-Baker, S.; Weller, M. T. *Solid State Ionics* **1986**, *18 & 19*, 89.
(22) Eda, K. *J. Solid State Chem.* **1989**, *83*, 292.
(23) Sotani, N.; Eda, K.; Kunitomo, M. *J. Chem. Soc., Faraday Trans.* **1990**, *86*, 1583.
(24) Eda, K. *J. Mater. Chem.* **1992**, *2*, 533.
(25) Eda, K.; Sukejima, A.; Matsuura, N.; Sotani, N. *Chem. Lett.* **1998**, 819.
(26) Sotani, N.; Shimada, I.; Suzuki, T.; Eda, K.; Kunitomo, M. *Solid State Ionics* **1998**, *113−115*, 377.
(27) Smith, R. L.; Rohrer, G. S. *J. Catal.* **1998**, *173*, 219.
(28) Smith, R. L.; Rohrer, G. S. *J. Catal.* **1999**, *184*, 49.
(29) Zeng, H. C.; Ng, W. K.; Cheong, L. H.; Xie, F.; Xu, R. *J. Phys. Chem. B* **2001**, *105*, 7178.
(30) Balakumar, S.; Zeng, H. C. *J. Cryst. Growth* **1998**, *194*, 195.
(31) (a) Ji, L.; Lin, J.; Zeng, H. C. *J. Phys. Chem. B* **2000**, *104*, 1783. (b) Xu, Z. P.; Zeng, H. C. *J. Phys. Chem. B* **2001**, *105*, 1743.
(32) (a) Leung, Y. L.; Wong, P. C.; Zhou, M. Y.; Mitchell, K. A. R.; Smith, K. J. *Appl. Surf. Sci.* **1998**, *136*, 178. (b) Kono, M.; Wong, P. C.; Li, Y. S.; Mitchell, K. A. R. *Surf. Rev. Lett.* **2000**, *7*, 227.

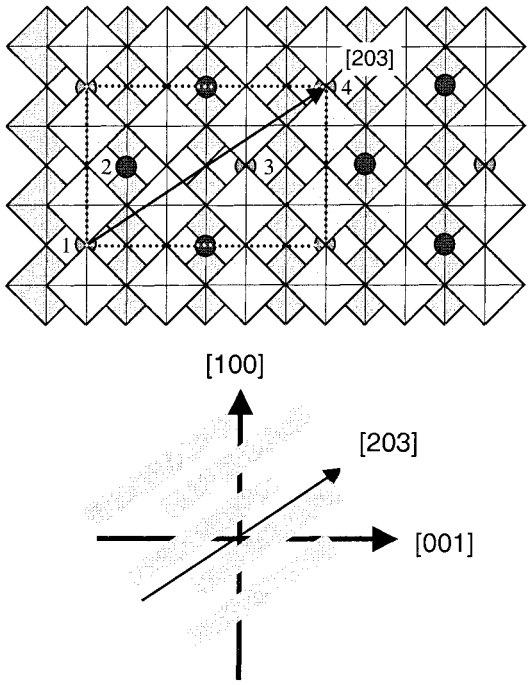

Figure 1. Schematic illustration of the α-MoO_3 double-layered structure and crystal orientations. Light gray squares indicate the MoO_6 octahedra in the top sublayer while the darker squares represent the bottom sublayer. Hydrogen atoms are shown as dark dots underneath or above the bridging oxygen (oxygen atoms are not shown).

tal samples change their color from light lemon yellow to blue, a typical color known for hydrogen molybdenum bronze.[24,33] The crystal structure and orientations of this bronze phase on the (010) surface are illustrated in Figure 1. To have an actual view, Figure 2 shows two α-MoO_3 single-crystal samples on which acicular H_xMoO_3 crystallites ($x \approx 0.33$, orthorhombic, $a = 3.89$ Å, $b = 14.06$ Å, and $c = 3.74$ Å,[33] XRD results) are formed topotactically as they protrude directly from the {010} surfaces. The formation of the crystallites starts at a temperature as low as 125 °C. These needlelike crystallites with their orientations along ⟨203⟩ have a few tens of nanometers in width and up to a few tens of micrometers in length. Our cross-sectional analysis shows that the average height of the rising crystallites is about 0.7 nm (Figure 2a), which is equivalent to the thickness of one double layer (or $^1/_2b$). As shown in Figure 2a, interestingly, a maze is formed from these crystallites which are parallel along ⟨203⟩. As the crystallites have not been "glued" together (i.e., the entrances of each partition are still open), it is believed that the hydrogen atoms ("mice") at this stage can still travel freely in the interlayer space from one partition to the other. Therefore, the walls of growing crystallites have the same dimension (thickness) because of having the same chance in the growth when diffusion of the guest species is not a problem. With prolonged growth, the width of the crystallites increases (e.g., up to ≈150 nm in Figure 2b), as indicated by sharp boundaries. Furthermore, the crystallites now bump into each other. The openings of the partitions are being narrowed, and some of them have been entirely closed. The hydrogen atoms in the interlayer space are no longer as free as before, and the variation in wall thickness can be clearly observed now. For example, the small crystallites (marked with A and B in Figure 2b) confined within a partition are particularly thin due to the limited entrance for hydrogen atoms. The average height of these crystallites now is about 1.4 nm (the thickness of two double layers, i.e., *b*), as revealed in the cross-sectional analysis in Figure 2b. By comparing the lattice parameter *b* of α-MoO_3 with that of H_xMoO_3, the dimension of the formed H_xMoO_3 in the *b*-axis can be deduced,[27,28] which is about 50 and 100 nm in a and b, respectively, of Figure 2, based on the data of cross-sectional analysis.

Although the insertion direction of a proton into the α-MoO_3 is now known along ⟨001⟩ directions,[29] it is still not clear whether the surface stress may also generate some entrance points (with higher surface energy) for hydrogen on the {010} planes. For example, in an earlier AFM investigation on the reaction between α-MoO_3 and $CH_3OH + N_2$, it has been found that H_xMoO_3 crystallites form preferentially on the surface defects (i.e., at the edges of surface pits on {010}).[28] In particular, it has been observed that the total volume of H_xMoO_3 crystallites formed on the pitted surface is about 10 times larger than that formed on the ideally flat surface.[28] There are two possible causes responsible for the observed preferential growth: (1) the surface pits may provide more entrance points for hydrogen to enter along the ⟨001⟩ directions and (2) the surface pits may exert certain structural stress on {010} planes which in turn serve as nucleation sites (e.g., pit edges) for the growth of acicular H_xMoO_3. To figure out these possible causes, in the present work, α-MoO_3 single-crystal samples embedded with nanometer-scale α-MoO_3 crystallites (e.g., tiny light dots in Figure 2) on {010} planes were selected. These nanocrystallites were deposited (or embedded) onto {010} planes due to a sudden change in melt temperature during high-temperature solution growth,[30,34] and they will in principle create mechanical and structural stresses on the {010} planes underneath. Nonetheless, the nanocrystallites neither provide entrance points of hydrogen nor act as nucleation sites for the H_xMoO_3 to grow because no clear relationship between them can be found. Therefore, the growth of H_xMoO_3 is independent of the surface stress on {010} planes but dependent on the openness of the maze entrance in the interlayer space. The above new experimental findings are in excellent agreement with our previous observation on proton insertion mode along ⟨001⟩ directions.[29]

The actual position of protons in H_xMoO_3 has been investigated with inelastic neutron scattering and proton NMR methods, and it has been known that they are attached to bridging oxygen atoms of an α-MoO_3 double layer (i.e., to the intrasheet zigzag chain) at this hydrogen content ($x = 0.23-0.40$).[19−21,23,35] Regarding the growth directions along ⟨203⟩, Figure 1 depicts a double-layer structure of α-MoO_3 with a proton content $x = 0.33$. As can be understood, cationic repulsion among the protons is a major driving force for this low proton-content growth. By directing protons along ⟨203⟩, maximum distances between two protons can be

(33) Birtill, J. J.; Dickens, P. G. *Mater. Res. Bull.* **1978**, *13*, 311.

(34) Zeng, H. C. *J. Crystal Growth* **1998**, *186*, 393.

(35) Ritter, C.; Müller-Warmuth, W.; Schollhorn, R. *J. Chem. Phys.* **1985**, *83*, 6130.

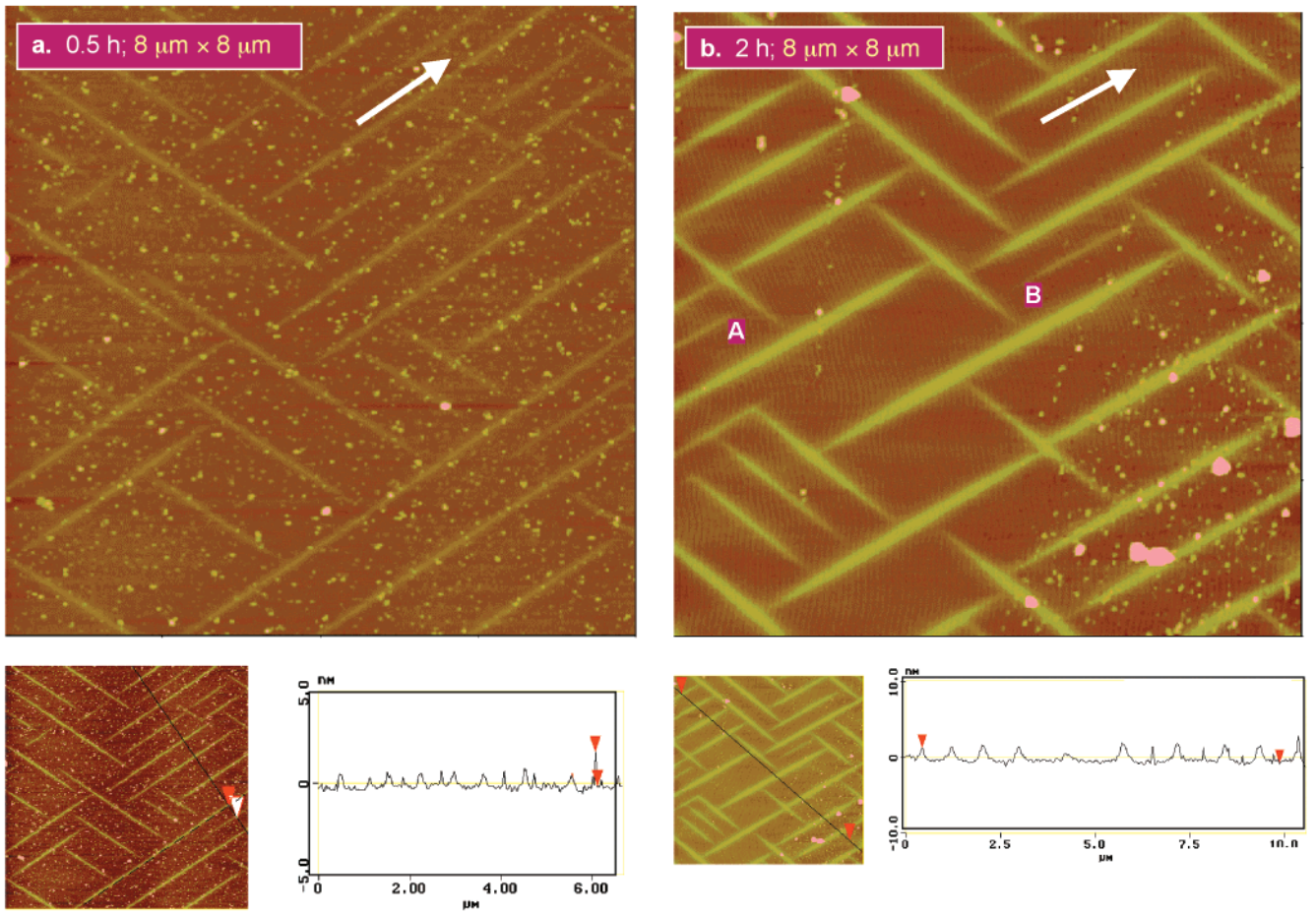

Figure 2. (a) AFM image and sectional analysis of a α-MoO_3 single crystal after 0.5 h of reaction in $H_2S + H_2$ (20 mL/min; H_2S = 5 mol %) at 152 °C; (b) AFM image and sectional analysis of a α-MoO_3 single crystal after 2 h of reaction in $H_2S + H_2$ (20 mL/min; H_2S = 5 mol %) at 152 °C. Needlelike H_xMoO_3 crystallites are along ⟨203⟩ directions. (The white arrow indicates [203] direction.) And the little light spots are as-grown α-MoO_3 nanocrystallites on the (010) surface (see the text).

achieved; such positions are indicated by (1), (2), (3), and (4) in Figure 1.

The insertion reactions at a temperature around 150 °C for H_xMoO_3 formation do not change the surface oxidation states of Mo significantly using a $H_2S + H_2$ stream. As reported in our previous XPS study,[29] there are only two surface species of molybdenum, one assigned to the unreacted MoO_3 single crystal (BE of Mo $3d_{5/2}$ = 232.5 eV) and the other to H_xMoO_3 (BE of Mo $3d_{5/2}$ = 231.3 eV), whose assignments will be further addressed shortly. The photoelectron peak area ratios arising from the above two surface phases are about equal to their actual surface area ratios. For example, the peak area ratio of Mo 3d (H_xMoO_3) to Mo 3d (MoO_3) is 8% for the sample reported in Figure 2b, which is approximately equal to the surface area ratio revealed by the AFM method.

From Acicular H_xMoO_3 To Block H_xMoO_3. After the formation of maze structure, the growth of needlelike H_xMoO_3 at ≈150 °C is apparently slowed, as the entrance to each partition becomes a controlling factor for proton insertion. Nonetheless, with an increase in reaction temperature, the growth of H_xMoO_3 crystallites continues. Figure 3 displays two α-MoO_3 single-crystal samples after reactions in H_2S/H_2 at 300 °C. As can be seen, the growth of H_xMoO_3 (light areas) perpendicular to ⟨203⟩ is significant at this reaction temperature. With a longer reaction time (1 h vs 1.5 h), the darker areas in these two images (i.e., previously unreacted α-MoO_3 crystal areas at ≈150 °C, Figure 2) are narrowed, indicating a transformation from acicular H_xMoO_3 to block H_xMoO_3. Because of differences in lattice parameters for H_xMoO_3 and α-MoO_3, the crystal surfaces are severely buckled. Although the light-to-dark contrasts in these images can be as big as 14−15 nm, the hill-to-valley transition (i.e., H_xMoO_3 to α-MoO_3 transition) is rather smooth, as shown in the section profile curves. Furthermore, the section analysis shows that narrow dips (the lighter brown strips in Figure 3) within a big H_xMoO_3 block still have a height difference of 1−2 nm (see the black profile curves in Figure 3), whose magnitude is essentially the same as those reported in Figure 2. Even the insertion reaction occurs at a higher temperature now; we believe the temperature rise does not alter the hydrogen insertion mode along ⟨001⟩ because all our AFM images show no connection between the α-MoO_3 nanocrystallites on {010} surfaces and preferential H_xMoO_3 growth, as discussed in the previous subsection.

In Figure 4, the new diffraction patterns after reactions in H_2S/H_2 at 300 °C are clearly departed from the original α-MoO_3 pattern, noting that the new patterns become more intense while that of α-MoO_3 is getting weaker. In particular, the (0*k*0) peaks are shifted to the left-hand side of 2θ, which indicates an expansion of inter-double-layer distance (in *b*-axis) when protons are

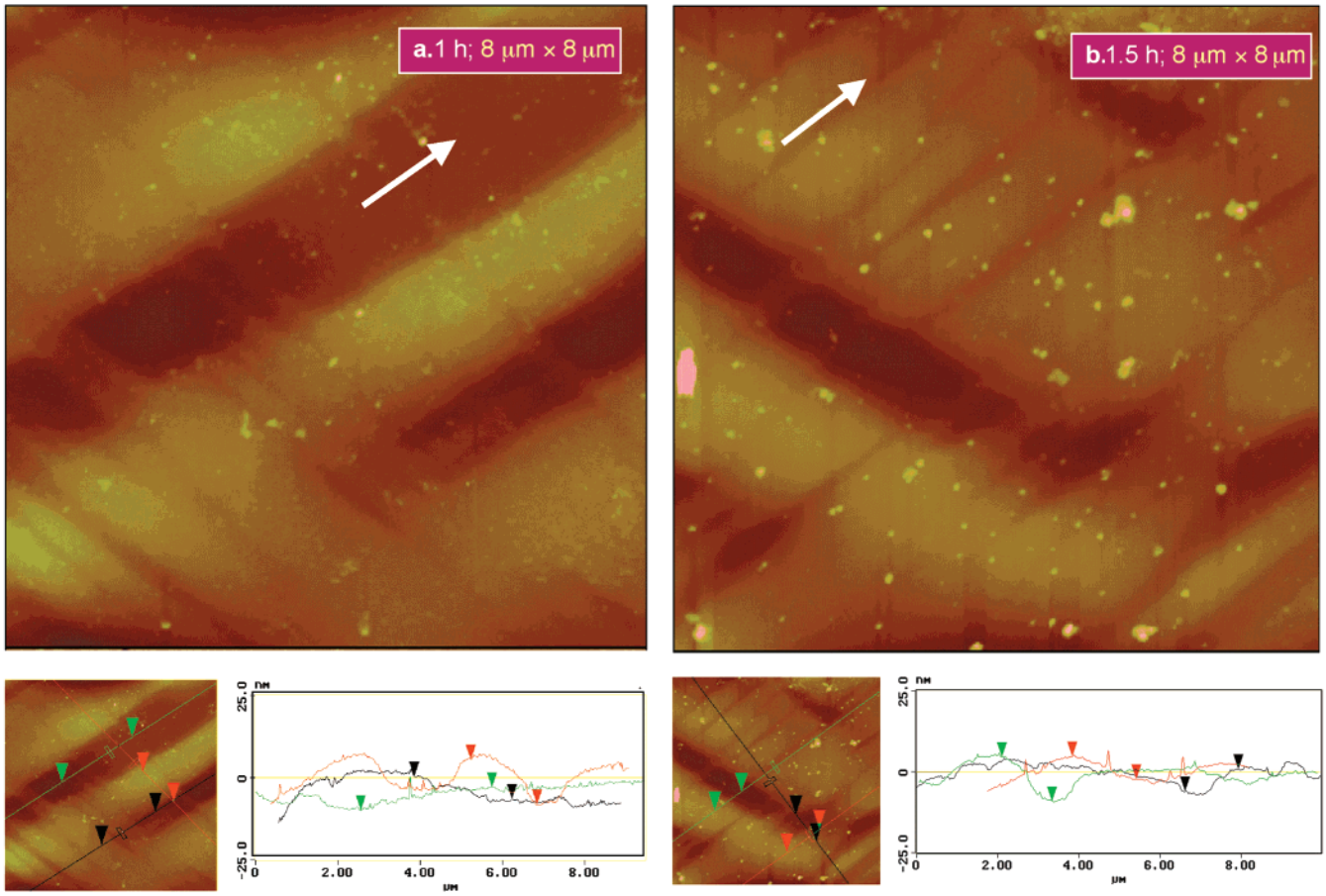

Figure 3. (a) AFM image and sectional analysis of an α-MoO_3 single crystal after 1 h of reaction in $H_2S + H_2$ (20 mL/min; H_2S = 5 mol %) at 300 °C; (b) AFM image and sectional analysis of an α-MoO_3 single crystal after 1.5 h of reaction in $H_2S + H_2$ (20 mL/min; H_2S = 5 mol %) at 300 °C. The white arrow indicates [203] direction, and the little light spots are as-grown α-MoO_3 nanocrystallites on the (010) surface (see the text).

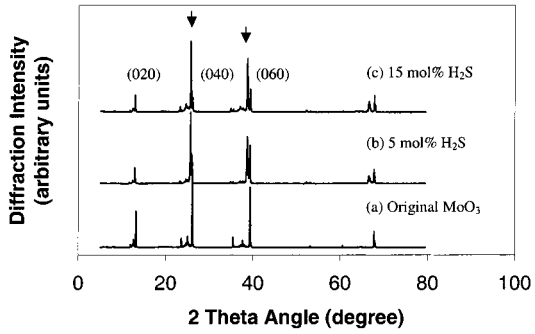

Figure 4. XRD patterns for (a) an as-grown α-MoO_3 single-crystal sample, (b) a sample after 1.5 h of protonation in a $H_2S + H_2$ stream (20 mL/min; H_2S = 5 mol %) at 300 °C, and (c) a sample after 1.5 h of protonation in a $H_2S + H_2$ stream (20 mL/min; H_2S = 15 mol %) at 300 °C. Arrows indicate some pronounced peaks of $H_{0.3}MoO_3$ phase.

intercalated. The XRD structural analysis reveals that the H_xMoO_3 (both acicular and block crystallites) belongs to a *C*-centered orthorhombic cell with lattice parameters of $a = 3.89$ Å, $b = 14.06$ Å, and $c = 3.74$ Å, identical to the reported data for the hydrogen molybdenum bronze phase H_xMoO_3 with $x = 0.23-0.40$.[33]

Regarding the role of reactants in a gas stream, H_2S is believed to be the proton source for the formation of H_xMoO_3 rather than H_2 because it has been reported that protonation does not take place when α-MoO_3 {010} cleavage surfaces are reacted with a 10 mol % H_2 (balanced with N_2) gas stream over 200−400 °C.[27] Unlike those at low temperatures for needlelike H_xMoO_3 (Figure 2), nonetheless, reactions using the $H_2S + H_2$ gas stream at higher temperatures for H_xMoO_3 blocks (Figure 3) cause a certain degree of sulfidation on sample surfaces. Figure 5 reports our XPS surface analysis for two α-MoO_3 crystal samples after protonation reactions at 300 °C. Adsorption of atmospheric CO_2 does not occur on the reacted samples because C 1s BE = 289.0−289.5 eV for CO_3^{2-} surface species is not detected (C 1s at 284.7 eV is assigned to adventitious carbons).[36] Deconvolution results of the Mo 3d doublet indicate the presence of two chemical species of Mo on the surfaces, noting that the small peaks at BE ≈ 225.4 eV in the Mo 3d spectra belong to the S 2s core level.[36] The first doublet at Mo $3d_{5/2}$ ≈ 228.4 eV is attributed to the formation of MoS_2 on the surface region (because these BEs are in good agreement with the literature data for MoS_2) while the second doublet at Mo $3d_{5/2}$ = 230.9−231.7 eV can be assigned to the surface H_xMoO_3 phase.[29,37] The Mo $3d_{5/2}$ assigned for H_xMoO_3 implies an oxidation state of Mo greater than 5 but smaller than 6. Indeed, our observed data here fall well between the

(36) Moulder, J. F.; Stickle, W. F.; Sobol, P. E.; Bomben, K. D. *Handbook of X-ray photoelectron spectroscopy: a reference book of standard spectra for identification and interpretation of XPS data*; Chastain, J., Ed.; Perkin-Elmer Corporation, Physical Electronics Division; Imprint: Eden Prairie, Minneapolis, MN, 1992.

(37) Specvack, P. A.; McIntype, N. S. *J. Phys. Chem.* **1992**, *96*, 9029.

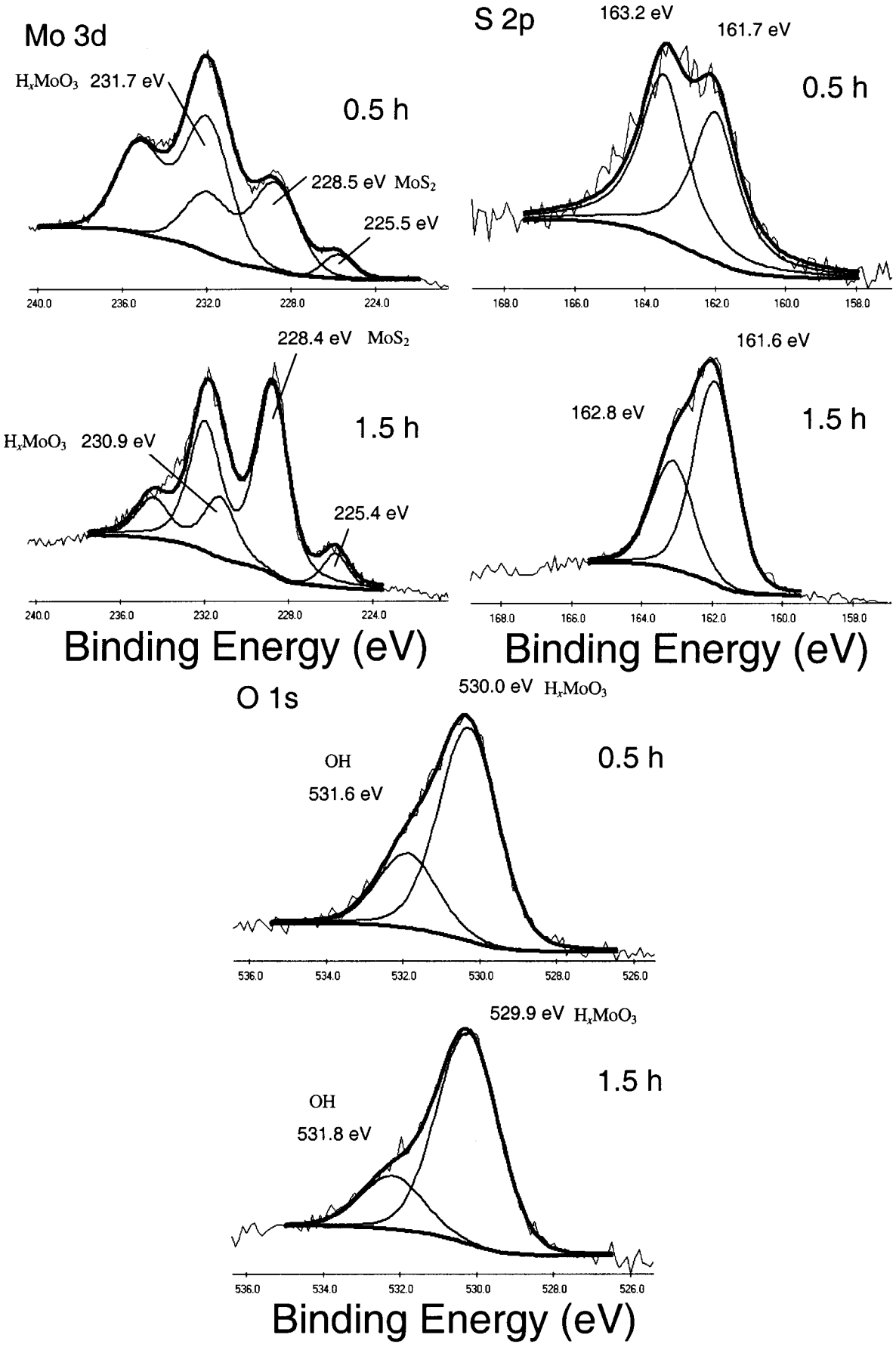

Figure 5. XPS spectra of Mo 3d, S 2p, and O 1s for two α-MoO_3 single-crystal samples reacted in a $H_2S + H_2$ stream (20 mL/min; H_2S = 15 mol %) at 300 °C for 0.5 and 1.5 h, respectively.

BEs of Mo 3d for these two oxidation states. It has been widely reported in the literature that Mo^{5+} in reduced MoO_3 has a BE of Mo $3d_{5/2}$ = 230.0−231.7 eV while Mo^{6+} in MoO_3 has a BE of Mo $3d_{5/2}$ = 232.0−232.7 eV.[7,37−40] More importantly, the growth of the MoS_2 doublet at Mo $3d_{5/2}$ = 228.5 eV [36,41−43] is clearly observed while the oxide doublet is shifted to a lower BE region with a longer reaction time (1.5 h), which is in line with the general expectation for Mo sulfidation/reduction in a reducing environment. The S 2p spectra also indicate an increase in MoS_2 surface phase with reaction time. The BE peaks at ∼161.6 eV are assigned to S $2p_{3/2}$ of S^{2-} while the peaks at 163.2−162.8 eV are assigned to S $2p_{1/2}$ of S^{2-} in MoS_2.[42,43] It should be mentioned that the latter peak at 163.2 eV (with a reaction time of 0.5 h) also contains deposited elemental sulfur which results from the dissociation reaction of H_2S during the formation of H_xMoO_3 and MoS_2 (on the surface only! see later discussion) in which Mo^{6+} is reduced by H_2S.[29,36] The elemental sulfur can be vaporized with a longer heating time; a thin layer of sublimated sulfur (yellowish) has been observed on the top of the reactor after the experiments at 300 °C. Furthermore, well-defined spin−orbit-splitting of the S 2p doublet, identical to those reported in the literature,[42,43] can be observed for the sample after reacting at this temperature for 1.5 h. The above assignments are further supported by our analytical results of the O 1s core level. The O 1s peaks at ∼529.9 eV are assigned to the lattice oxygen in the H_xMoO_3 phase and the peaks at ∼531.7 eV to the oxygen in surface hydroxyl groups resulting from chemisorption reaction between the terminal oxygen of the double layer and dissociated hydrogen species.[17,36,44,45] The intensity of hydroxyl component in the O 1s core level reduces when the surface of H_xMoO_3 decreases (i.e., it is converted to MoS_2) with a prolonged reaction time (1.5 h). This XPS correlation reveals that the surface hydroxyl groups are indeed associated to H_xMoO_3, not to MoS_2.

It should be pointed out that the formation of MoS_2 occurs merely on the topmost surface, noting that no bulk phase MoS_2 is detectable in our XRD study for the samples prepared under similar experimental conditions but with an even longer reaction time or higher H_2S concentration (refer to the XRD results in Figure 4). Regarding the conversion of MoS_2 from H_xMoO_3 and α-MoO_3, it is noted that the specific areas per Mo atom in the basal planes of these three compounds are 8.65 Å^2/Mo (MoS_2), 7.27 Å^2/Mo (H_xMoO_3), and 7.32 Å^2/Mo (α-MoO_3), respectively. Because of a small variation of the specific areas (within 16%), it is suggested that surface sulfidation/reduction processes of H_xMoO_3 and α-MoO_3 to MoS_2 at 300 °C should not cause a substantial mass relocation of Mo cations between different basal planes. In this agreement, the topographical investigation shown in Figure 3 also indicates there is no reconstruction (such as formation of triangular/hexagonal crystallite with 2H−MoS_2 structure), and the surface blocks still align along ⟨203⟩ orientations that belong to the original H_xMoO_3 and α-MoO_3 phases (see Figures 2 and 3).

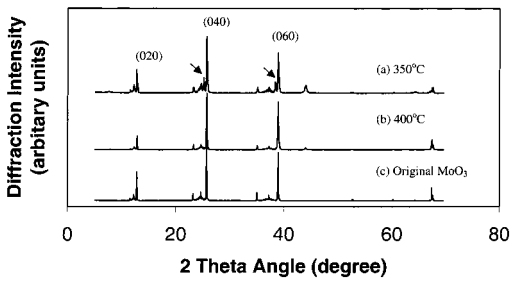

Figure 6. XRD patterns for (a) a sample after 1 h of protonation in a $H_2S + H_2$ stream (20 mL/min; H_2S = 15 mol %) at 300 °C and then 1 h of deprotonation in air at 350 °C, (b) a sample after 1 h of protonation in a $H_2S + H_2$ stream (20 mL/min; H_2S = 15 mol %) at 300 °C and then 1 h of deprotonation in air at 400 °C, and (c) an as-grown α-MoO_3 single-crystal sample. Arrows indicate some pronounced peaks of $H_{0.3}MoO_3$ phase.

Removal of Protons from H_xMoO_3. On the basis of the observed lattice parameters, it is clear that the formation H_xMoO_3 structure involves the α-MoO_3 contraction along ⟨100⟩ directions (a = 3.963−3.89 Å, or −1.8%), and expansions along both ⟨010⟩ (b = 13.86−14.06 Å, or +1.4%) and ⟨001⟩ (c = 3.696−3.74 Å, or +1.2%). The structural stress of the samples caused by the proton insertion will be gradually increased when the narrow H_xMoO_3 crystallites are developed into blocks, which converts most of α-MoO_3 into H_xMoO_3 phase. On the other hand, these intraplanar and interplanar stresses may be released when the guest species hydrogen is removed. In the present work, the removal of a proton (oxidation) in the H_xMoO_3 blocks was carried out at 350−400 °C in static laboratory air (Table 1). In Figure 6, two XRD patterns recorded for the samples after deprotonation reactions are displayed. Within 1 h of oxidation reaction at 350 °C, the pattern of the H_xMoO_3 phase has been significantly reduced. At 400 °C, the H_xMoO_3 phase can be completely converted to α-MoO_3 phase with the same reaction time; the oxidized sample indeed shows a typical lemon yellow color for the α-MoO_3 phase. It should be mentioned that the surface species MoS_2 on top of H_xMoO_3 and α-MoO_3 is also oxidized during this proton removal process. As the oxidative conversion of the MoS_2 basal layer to α-MoO_3 double layer is mainly an intraplanar shrinking process (the specific area of Mo = 8.65 Å^2/Mo in MoS_2 down to 7.32 Å^2/Mo in α-MoO_3), the oxidation process will not cause a vertical reconstruction among the different double layers stacked along the b-axis.

Nonetheless, the α-MoO_3 crystal host shows some appreciable morphological changes after the deprotonation/oxidation reactions. Quite unexpectedly, the dark

(38) Anwar, M.; Hogarth, C. A.; Bulpett, R. *J. Mater. Sci.* **1989**, *24*, 3087 and references therein.
(39) Delporte, P.; Meunier, F.; Pham-Huu, C.; Vennegues, P.; Ledoux, M. J.; Guille, J. *Catal. Today* **1995**, *23*, 251.
(40) Braun, S.; Appel, L. G.; Camorim, V. L.; Schmal, M. *J. Phys. Chem. B* **2000**, *104*, 6584.
(41) Thurston, T. R.; Wilcoxon, J. P. *J. Phys. Chem. B* **1999**, *103*, 11.
(42) Park, K. T.; Kong, J.; Klier, K. *J. Phys. Chem. B* **2000**, *104*, 3145.
(43) Liao, H.; Wang, Y.; Zhang, S.; Qian, Y. *Chem. Mater.* **2001**, *13*, 6.
(44) (a) Zemlyanov, D. Y.; Savinova, E.; Scheybal, A.; Doblhofer, K.; Schlogl, R. *Surf. Sci.* **1998**, *418*, 441. (b) Baird, T.; Campbell, K. C.; Holliman, P. J.; Hoyle, R. W.; Stirling, D.; Williams, B. P.; Morris, M. *J. Mater. Chem.* **1997**, *7*, 319. (c) McCafferty. E.; Wightman, J. P.; Cromer, T. F. *J. Electrochem. Soc.* **1999**, *146*, 2849. (d) Simmons, G. W.; Beard, B. C. *J. Phys. Chem.* **1987**, *91*, 1143. (e) Chernyshova, I. V.; Andreev, S. I. *Appl. Surf. Sci.* **1997**, *108*, 225.
(45) Hermann, K.; Michalak, A.; Witko, M. *Catal. Today* **1996**, *32*, 321.

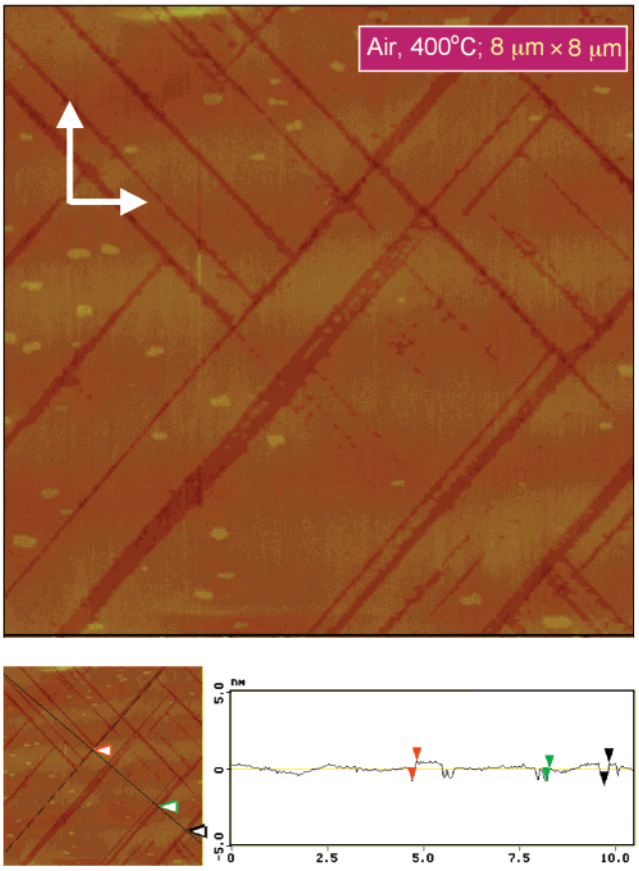

Figure 7. AFM image and step profile analysis of a α-MoO_3 single-crystal sample after both protonation and deprotonation reactions: 1.5 h of reaction in $H_2S + H_2$ (20 mL/min; H_2S = 15 mol %) at 300 °C and then 2 h of oxidation at 400 °C in static air. The white arrows indicate [100] (vertical) and [001] (horizontal) directions, and the little light spots are as-grown α-MoO_3 nanocrystallites on the (010) surface (see the text).

boundaries among the H_xMoO_3 blocks (Figure 3) along ⟨203⟩ directions are no longer observable in all our deprotonated α-MoO_3 samples (more than 10 samples). Instead, they are replaced by thin concave boundaries along ⟨101⟩ directions. Figure 7 reports the surface topography of a deprotonated α-MoO_3 crystal sample. Surprisingly, the surface buckling (Figure 3) disappears when the hydrogen is removed, which indicates a high elasticity of these layered compounds as host materials. As can be seen, the (010) surface is divided into tilted rectangles with various sizes bounded with {101} planes. The inter-crystallographic-plane angles between $(\bar{1}01)$ and (101) planes and between (101) and $(10\bar{1})$ planes of α-MoO_3 are 94° and 86°, respectively,[46] which can be clearly observed in Figure 7. More interestingly, the heights of these α-MoO_3 surface blocks are typically at 1 or 2 double-layer thickness (0.69 or 1.38 nm), which is evidenced in the height profile analysis (e.g., the lower part of Figure 7). It has been reported that the removal of protons from H_xMoO_3 in oxygen-free atmospheres (such as N_2) will give rise to water molecules and a defective MoO_3 host structure (MoO_{3-x} to be exact) due to the removal of lattice oxygen.[24] On the other hand, the positive weight gain of oxygen in defective MoO_{3-x} powder samples upon heating with air has been proven

(46) Balakumar, S.; Zeng, H. C. *J. Cryst. Growth* **1999**, *197*, 186.

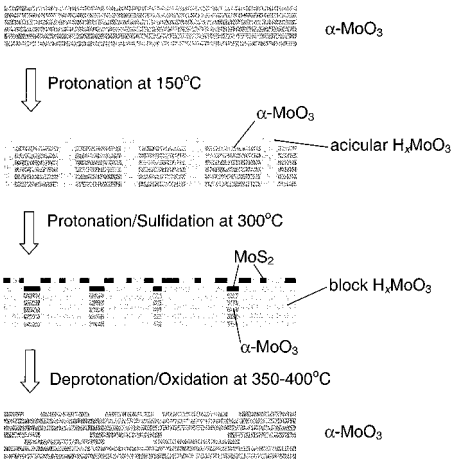

Figure 8. Schematic illustration of the protonation/sulfidation and deprotonation/oxidation processes; the number of total double layers has been fixed at 6 in this illustration and inter-basal-layer-spacings for different compounds are not drawn according to their actual proportions.

with TGA/DTA methods, which indicates that this oxidation process is exothermic.[24] In our current case, the oxidation reaction with air not only helps molybdenum restore its VI oxidation state but also eliminates the structural stresses among the H_xMoO_3 blocks by removing intercalated hydrogen. It is clear that air also mediates the oxygen-anionic defects in the boundaries among the H_xMoO_3 blocks because there is no such structural deformation (the deep valleys in Figure 3) along ⟨203⟩ directions of the α-MoO_3 crystal.

To address the above α-MoO_3 block formation on the surface upon proton removal, Figure 8 depicts a schematic summary based on the findings of this work. The introduction of protons into the α-MoO_3 lattice pushes the double layer upward. Depending on the degree of protonation, the extruding H_xMoO_3 needles/blocks can be a few (typically 1 or 2) double layers above the original α-MoO_3 {010} plane level, as reported in the cases of Figure 3. When the H_xMoO_3 phase is deprotonated, the double layers of the H_xMoO_3 phase simply rejoin the nearest neighboring double layers of the α-MoO_3 phase (Figure 8), leaving the extruding double layer(s) laterally unattended. These surface α-MoO_3 double layers later reorient themselves along ⟨101⟩ directions under heating conditions (350−400 °C) because the surface energy of {101} planes is lower, compared to that of {203} planes.[46]

Conclusions

In summary, acicular and block crystallites of H_xMoO_3 ($x \approx 0.33$) can be generated on the (010) surface of an α-MoO_3 single crystal respectively at 125−152 and 300 °C in a H_2S/H_2 atmosphere. Even with the presence of nanocrystallites on the (010) surface of α-MoO_3, the H_xMoO_3 needles and blocks are still only grown along ⟨203⟩ and/or their perpendicular directions, which indicates that the hydrogen insertion is irrespective of the defects and stress on the surface of a basal plane. This finding further reconfirms our previous observation that the hydrogen enters along ⟨001⟩ directions of the crystal. When the needlelike crystallites (along ⟨203⟩ directions) are grown into the larger block forms, the crystal

surfaces are severely buckled due to the insertion of hydrogen. The insertion of hydrogen at 300 °C is also accompanied with a certain degree of sulfidation that forms MoS_2 on the outmost surface layer, although no further reconstruction is observed. At 350−400 °C, the block H_xMoO_3 and surface MoS_2 can be converted efficiently back to α-MoO_3 phase in laboratory air. Interestingly, the deprotonated α-MoO_3 shows formation of surface blocks bordered with {101} planes. The heights of these surface blocks are typically at 1 or 2 double-layer thickness, which can be traced back to their original heights of H_xMoO_3 extrusion. It is clear that the deprotonation reactions with air at 350−400 °C not only cause debuckling of basal plane but also mediate the defects along ⟨203⟩ created during the protonation. The reversibility of protonation/deprotonation in α-MoO_3 is thus illustrated in detail in the present study.

Acknowledgment. The authors gratefully acknowledge the financial support of this research by the Ministry of Education, the National Science and Technology Board of Singapore, and the Natural Sciences and Engineering Research Council of Canada. The authors would also like to thank Mr. L. H. Cheong and Mr. W. K. Ng for providing technical assistance in AFM measurement.

CM011506Z